External corrosion modeling for an underground natural gas pipeline using COMSOL Multiphysics

Wadie Chalgham[*1†], Keo-Yuan Wu[*2], Ali Mosleh[1]
1. Mechanical and Aerospace Engineering Department, University of California, Los Angeles (UCLA)
2. Materials Science and Engineering Department, University of California, Los Angeles (UCLA)
* These authors are both first authors and contributed equally to this work
† Contact author: wadie.chalgham@ucla.edu

Abstract: This paper studies external corrosion of an underground transmission pipeline carrying natural gas. Pitting corrosion and Stress Corrosion Cracking (SCC) are two most common external corrosion types for buried pipelines and they usually happen when the mitigation methods such as coating or impressed current cathodic protection (ICCP) fails or deteriorates. Pitting corrosion is a localized corrosion which occurs at sites with no coating or cathodic protection as a result of electrochemical reaction between the pipe material and a corrosive environment, while SCC is a joint action of a corrosive environment and tensile stress from the soil movement. A finite element model was developed in COMSOL Multiphysics to study the relationship between corrosion potential, current density, and von Mises stress along the corrosion defect as a result of near-neutral pH SCC using the Corrosion and Structural Mechanics Modules. On the other hand, pitting corrosion is simulated by the Caleyo et al.'s model, which calculates pit growth rate based on several operating inputs. Multiple sensitivity analyses were performed to find the relationship between the defect depth, defect length, and the soil stress with respect to anodic current density, cathodic current density, and corrosion potential in order to obtain corrosion rate for SCC. In addition, a demonstration of the pitting corrosion was performed by predicting pitting corrosion rate and depth given soil and pipe characteristics such as the soil resistivity, bicarbonate ions concentration ($[HCO^{3-}]$), pH level of the soil, chloride ions concentration ($[Cl^{-}]$), water content of the soil, sulphate ions concentration ($[SO4^{2-}]$), pipe/soil potential, bulk density of the soil, and redox potential. The SCC results show that the maximum corrosion potential decreases with the increasing defect depth, but increases with increasing defect length, and that the maximum von Mises stress increases with increasing defect depth but decreases with increasing defect length, which indicates that the corrosion is most severe at the center of the defect. The results of SCC and pitting corrosion models will be the input to a Bayesian Network model for external corrosion which calculates the probability of pipeline failure in terms of external corrosion. This model is composed of three layers, namely corrosion, mechanical, and reliability models. The corrosion models include pitting corrosion and stress corrosion cracking. The output of this model will be the corrosion depth based on the corrosion rate results of this paper. The mechanical model calculates the remaining strength of the pipe given the dimension of the defects and will be used in the reliability model for the probability of the pipeline failure calculation.

Keywords: External Corrosion, Natural Gas Pipeline, Pitting Corrosion, SCC, Bayesian Network, Structural Health Monitoring

1. Introduction

Operational and management complexity of pipelines has significantly increased due to the rapid growth of oil and gas industry. Extreme operating conditions and adverse environment often lead to corrosion problems and tremendous consequences on the pipelines [1]. Therefore, more efforts have been dedicated to ensuring the integrity of the infrastructure. With the aid of IoT technology, in-situ pipeline health monitoring facilitates reliable risk assessment which provides optimal mitigation and maintenance actions to take based on the pipeline health condition. To meet that demand, the authors have been developing a pipeline health monitoring and management web application that can integrate the data, methods, and technologies into a dynamic pipeline heath monitoring system supported by multiple probabilistic predictive models [2]. These models include dynamic hybrid causal logic, corrosion prognosis, and sensor placement optimization models. Corrosion prognosis function requires the development of corrosion predictive models. A natural gas pipeline can suffer both internal and external corrosion as shown in Figure 1. One of the major threat to the gas pipelines is internal corrosion, which can take place in the form of uniform corrosion [3], pitting corrosion [4], erosion corrosion [5], microbiologically-influenced corrosion [6], and corrosion fatigue [7] depending on the operating and environmental conditions. Corrosive environment as a result of the presence of CO_2, H_2S, Cl^-, solids, and bacterial activities in the pipelines is the main cause of internal corrosion.

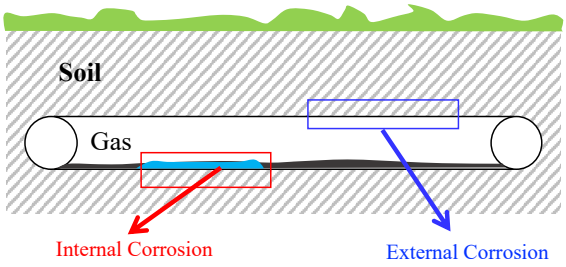

Figure 1. Internal and external corrosion can affect steel pipelines and create corrosion defects.

On the other hand, although the external pipeline surface is protected by coatings and cathodic protection most of the time, it is possible that coatings will degrade and cathodic protection will be broken due to many factors, leading to external corrosion. Pitting corrosion and Stress Corrosion Cracking (SCC) are regarded as two of common types of external corrosion, which take place due to the corrosive environment in soils and the longitudinal strain from the soil movement.

This paper aims at developing an external corrosion predictive model to fulfill the corrosion prognosis function for the developing pipeline health monitoring and management web application software. Pitting corrosion and SCC are both considered in the model. The model is a BN (Bayesian Network)-based model that enables the graphical demonstration of the whole system, the use of cause-effect relationships within the system, the consideration of uncertainties in data, the update with available monitoring data, and the integration of physics-based model, field data, and expert knowledge.

Detailed descriptions of both pitting corrosion and SCC models were provided. In this paper, COMSOL Multiphysics was used to develop a finite element model of SCC, and the results will be integrated into the external corrosion BN model. Finally, a case study was done to demonstrate the capability of the model.

2. Numerical Model

In this section, first the model of a pipeline is built in a modeling finite element software, COMSOL Multiphysics 5.3.
Figure 2 shows the overall geometry implemented for the numerical study. It shows that the model consists of a gas pipeline surrounded by soil. The electrolyte conductivity of soil domain is assumed to be 0.096 S/m.

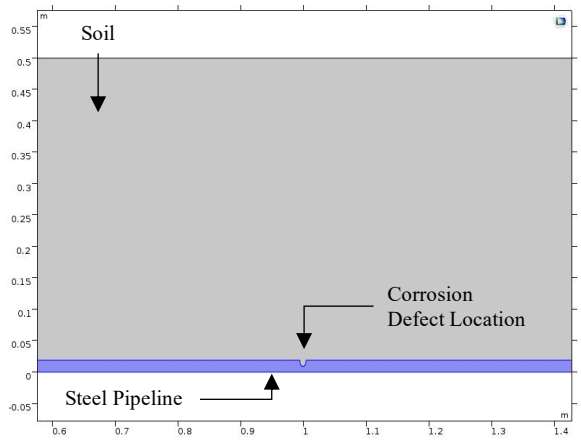

Figure 2. The model under study consists of a steel pipeline with a corrosion defect and surrounding soil.

The pipeline is made of high strength alloy steel and its material parameters are presented in Table A1 in the Appendix. The pipeline length is 1 m long with a wall thickness of 19.1 mm. The corrosion defect on the exterior side of the pipeline has an elliptical shape with a variable length and depth as shown in Figure 3.

The defect length is defined as the defect propagation at the surface of the pipe while the defect depth is defined as the distance from the pipe surface to deepest point the corrosion defect has reached in the vertical direction.

Initially, the defect length and depth are set to 1 mm and will be varied later on in order to perform a sensitivity analysis. The parameters and variables' values used in the simulations can be found in Tables A2 and A3 in the Appendix.

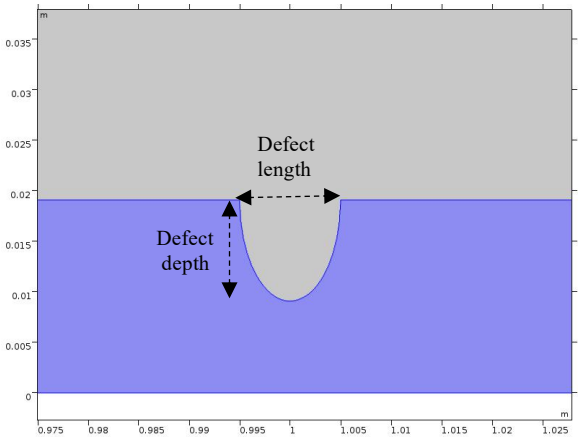

Figure 3. The corrosion defect has an elliptical shape with a variable length and depth.

3. Theory and Governing Equations

3.1 SCC

The model presented in this paper is used to study the behavior of SCC for underground gas pipelines subject to longitudinal strain caused by soil movement. Two electrochemical reactions, namely, steel oxidation for anodic reaction and hydrogen evolution for cathodic reaction, respectively are assumed to happen in a near-neutral pH environment.

3.1.1 Elastoplastic Stress

In this paper, elastoplastic stress is simulated over the steel pipeline based on the small strain plasticity model [8]. In this model, the isotropic hardening model is defined as:

$$\boldsymbol{\sigma_{yhard}} = \boldsymbol{\sigma_{exp}}\left(\boldsymbol{\varepsilon_p} + \frac{\boldsymbol{\sigma_e}}{\mathbf{E}}\right) - \boldsymbol{\sigma_{ys}} \qquad \text{(Eq. 1)}$$

where $\boldsymbol{\sigma_{yhard}}$ is the hardening function, $\boldsymbol{\sigma_{exp}}$ is the experimental stress-strain curve, $\boldsymbol{\varepsilon_p}$ is the plastic deformation, $\boldsymbol{\sigma_e}$ is the von Mises stress, **E** is the Young's modulus ($207\cdot10^9$ Pa), and $\boldsymbol{\sigma_{ys}}$ is the yield strength of high strength alloy steel ($806\cdot10^6$ Pa).
The experimental stress-strain curve used in the model is shown in Figure 4 and is prescribed in terms of a piecewise cubic interpolation function and is taken from [9].

3.1.2 Electrochemical Reactions

At the corrosion defect surface of pipelines, the two electrochemical reactions that could occur are: (1) the anodic (iron dissolution) reactions, and (2) the cathodic (hydrogen evolution) reactions. In this paper, it is assumed that the rest of pipeline surfaces are electrochemically inactive.

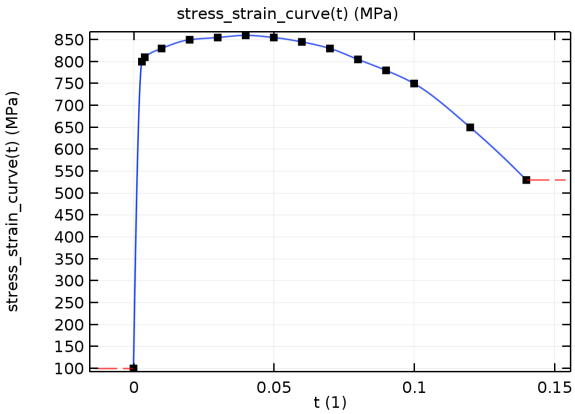

Figure 4. The experimental stress-strain curve.

In order to model the iron dissolution reaction, an anodic Tafel expression is used as follows:

$$\boldsymbol{i_a} = \boldsymbol{i_{0,a}}\,\mathbf{10}^{\frac{\eta_a}{A_a}} \qquad \text{(Eq. 2)}$$

where $\boldsymbol{i_a}$ is the local anodic current density, $\boldsymbol{i_{0,a}}$ is the exchange anodic current density ($2.353\cdot10^{-3}$ A/m^2), $\mathbf{A_a}$ is the Tafel slope (0.118 V) and $\boldsymbol{\eta_a}$ is the overpotential for the anodic reaction. $\boldsymbol{\eta_a}$ is found using Eq. 3 as follows:

$$\boldsymbol{\eta_a} = \emptyset_S - \emptyset_l - \boldsymbol{E_{eq,a}} \qquad \text{(Eq. 3)}$$

where $\boldsymbol{E_{eq,a}}$ is the equilibrium potential for the anodic reaction. $\boldsymbol{E_{eq,a}}$ is found using Eq. 4 as follows:

$$\boldsymbol{E_{eq,a}} = \boldsymbol{E_{eq0,a}} - \frac{\Delta P_m V_m}{zF} - \frac{TR}{zF}\ln\left(\frac{\nu\alpha}{N_0}\boldsymbol{\varepsilon_p} + \mathbf{1}\right) \qquad \text{(Eq. 4)}$$

where $\boldsymbol{E_{eq0,a}}$ is the standard equilibrium potential for the anodic reaction (−0.859 V), $\mathbf{\Delta P_m}$ is the excess pressure to elastic deformation ($2.687\cdot10^8$ Pa), $\mathbf{V_m}$ is the molar volume of steel ($7.13\cdot10^{-6}$ m^3/mol), **z** is the charge number for steel (2), **F** is the Faraday's constant, **T** is the absolute temperature (298.15 K), **R** is the ideal gas constant, **ν** is an orientation dependent factor (0.45), **α** is a coefficient ($1.67\cdot1015$ m^{-2}) and $\mathbf{N_0}$ is the initial dislocation density ($1\cdot1012$ m^{-2}).

In addition, in order to model the iron dissolution reaction, a cathodic Tafel expression is used as follows:

$$\boldsymbol{i_c} = \boldsymbol{i_{0,c}}\,\mathbf{10}^{\frac{\eta_c}{A_c}} \qquad \text{(Eq. 5)}$$

where $\boldsymbol{i_c}$ is the local cathodic current density, $\boldsymbol{i_{0,c}}$ is the exchange cathodic current density, $\mathbf{A_c}$ is the Tafel slope (−0.207 V) and $\boldsymbol{\eta_c}$ is the overpotential for the cathodic reaction. $\boldsymbol{\eta_c}$ is found using Eq. 6 as follows:

$$\boldsymbol{\eta_c} = \emptyset_S - \emptyset_l - \boldsymbol{E_{eq,c}} \qquad \text{(Eq. 6)}$$

where $\boldsymbol{E_{eq,c}}$ is the standard equilibrium potential for the cathodic reaction (−0.644 V). $\boldsymbol{i_{0,c}}$ is found using Eq. 7 as follows:

$$\boldsymbol{i_{0,c}} = \boldsymbol{i_{0,c,ref}}\,\mathbf{10}^{\frac{\sigma_e V_m}{6F(-A_c)}} \qquad \text{(Eq. 7)}$$

where $\boldsymbol{i_{0,c,ref}}$ is the reference exchange current density for the cathodic reaction in the absence of external stress/strain (1.457×10^{-2} A/m^2).

3.2 Pitting corrosion

3.2.1 Maximum pitting depth model

In order to simulate the pitting corrosion in buried gas pipelines, an empirical formula proposed by Velázquez et al. [10] is used. This model justifies its physical background by relating pit growth to soil and pipe characteristics with the multivariate regression analysis on observed corrosion data. Maximum pit depth as a function of time is described by a power law model shown as follows:

$$\mathbf{d_{max}(t) = \kappa(t - t_0)^{\alpha}} \quad \text{(Eq. 8)}$$

where $\boldsymbol{\kappa}$ is the pitting proportionality; $\boldsymbol{\alpha}$ is the exponent factor; $\mathbf{t_0}$ is the pitting initiation time.
The correlations between the pitting proportionality, the exponent factors, the soil, and pipe variables are shown as follows:

$$\boldsymbol{\kappa = \kappa_0 + \kappa_1 rp + \kappa_2 ph + \kappa_3 re + \kappa_4 cc + \kappa_5 bc + \kappa_6 sc} \quad \text{(Eq. 9)}$$

$$\boldsymbol{\alpha = \alpha_0 + \alpha_1 pp + \alpha_2 wc + \alpha_3 bd + \alpha_4 ct} \quad \text{(Eq. 10)}$$

where $\boldsymbol{\kappa_i}$ and $\boldsymbol{\alpha_i}$ are regression coefficients for the corresponding soil and pipe variables. Table 1 shows the soil and pipe variables, and Table 2 shows the regression coefficients of this model, respectively.

It should be noted that since the soil environments have large impact on the corrosion prediction, predicted model from one soil class is unreliable for the prediction in other soil classes. Therefore, the multivariate regression model provided here considers only the data from three different common soil classes, namely, clay, clay loam, and sandy clay loam.

Table 1. Soil and pipe characteristics

Variable	Symbol	Unit
Redox potential	rp	mV
pH	ph	-
Pipe-to-soil potential	pp	mV
Soil resistivity	re	Ω·m
Water content	wc	%
Soil bulk density	bd	g/mL
Chloride content	cc	ppm
Bicarbonate content	bc	ppm
Sulfate content	sc	ppm
Coating type	ct	-

Table 2. Pit initiation time and Regression coefficients for the maximum pitting depth model

Parameter (variable, symbol)	Value
$\boldsymbol{\kappa_0}$	6.08×10^{-1}
$\boldsymbol{\alpha_0}$	8.96×10^{-1}
$\boldsymbol{\kappa_1}$ (redox potential, rp)	-1.80×10^{-4}
$\boldsymbol{\kappa_2}$ (pH, ph)	-6.54×10^{-2}
$\boldsymbol{\kappa_3}$ (resistivity, re)	-2.60×10^{-4}
$\boldsymbol{\kappa_4}$ (chloride, cc)	8.74×10^{-4}
$\boldsymbol{\kappa_5}$ (bicarbonate, bc)	-6.39×10^{-4}
$\boldsymbol{\kappa_6}$ (sulphate, sc)	-1.22×10^{-4}
$\boldsymbol{\alpha_1}$ (pipe/soil potential, pp)	5.19×10^{-1}
$\boldsymbol{\alpha_2}$ (water content, wc)	4.65×10^{-4}
$\boldsymbol{\alpha_3}$ (bulk density, bd)	-9.90×10^{-2}
$\boldsymbol{\alpha_4}$ (coating type, ct)	4.31×10^{-1}

3.2.1 Pitting rate model

The observed pitting corrosion depth is the result of accumulation effect by the pitting corrosion rate as a function of time [11]. Therefore, taking time derivative of the maximum pitting depth model leads to the pitting rate model shown as follows:

$$\mathbf{v_m(t) = \kappa'(t - t_0)^{\alpha'}} \quad \text{(Eq. 11)}$$

where $\boldsymbol{\alpha' = \alpha - 1 < 1.0}$ and $\boldsymbol{\kappa' = \kappa\alpha}$.

3.3 Bayesian Belief Network

Bayesian Network (BN) provides a graphical representation of causal dependencies of a chain of variables in a probabilistic framework. For example, a chain of operating conditions leading to corrosion and finally to failure is a BN in this paper. It allows the calculation of the conditional probability of numerous interconnected parameters based on the Bayes theorem as shown in Eq. 12:

$$\mathbf{P(H_j|E)} = \frac{\mathbf{P(E|H_j)P(H_j)}}{\sum_{i=1}^{n} \mathbf{P(E|H_i)P(H_i)}} \quad \text{(Eq. 12)}$$

where $\mathbf{P(H_j|E)}$ is the posterior probability of event $\mathbf{H_j}$ given the observation $\mathbf{E}$; $\mathbf{P(H_j)}$ is the prior probability of the event $\mathbf{H_j}$ before the observation $\mathbf{E}$; $\mathbf{P(E|H_j)}$ is the likelihood function and is the probability of the observation $\mathbf{E}$ given that event $\mathbf{H_j}$ occurred; $\sum_{i=1}^{n} \mathbf{P(E|H_i)P(H_i)}$ is the sum of all the conditional probabilities of $\mathbf{E}$ given events $\mathbf{H_i}$ multiplied by the probabilities of $\mathbf{H_i}$.

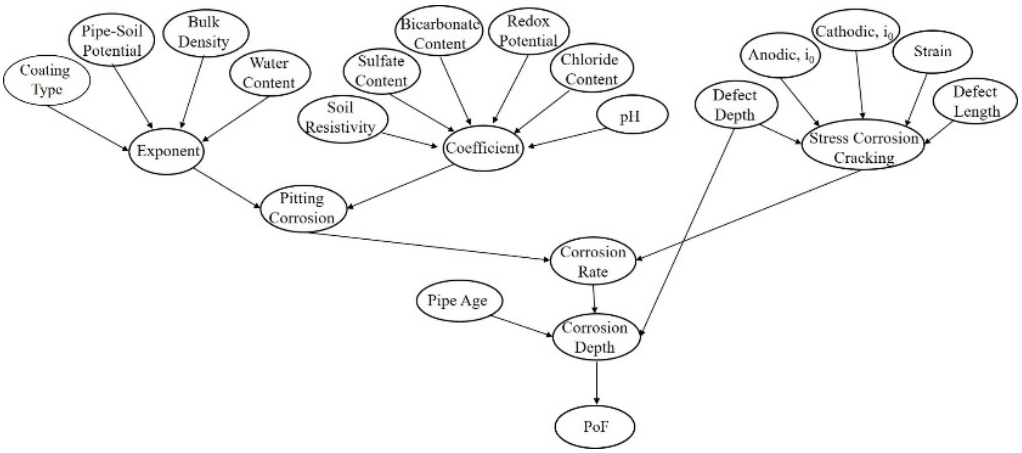

Figure 5. BBN model of external corrosion for a natural gas pipeline.

External corrosion for a natural gas pipeline is simulated by integrating two most common corrosion types, namely, pitting and SCC into a BN model. The BN of external corrosion is shown in Figure 5. Note that every node is linked to the next by cause-consequence relationships.

The quantification of the conditional probability tables was done based on the corrosion models, expert knowledge, and literature data. The details of each discretized node of the BN model are described in the authors previous work [2]. In this paper, the application of this model is demonstrated on an underground natural gas pipeline as a case study.

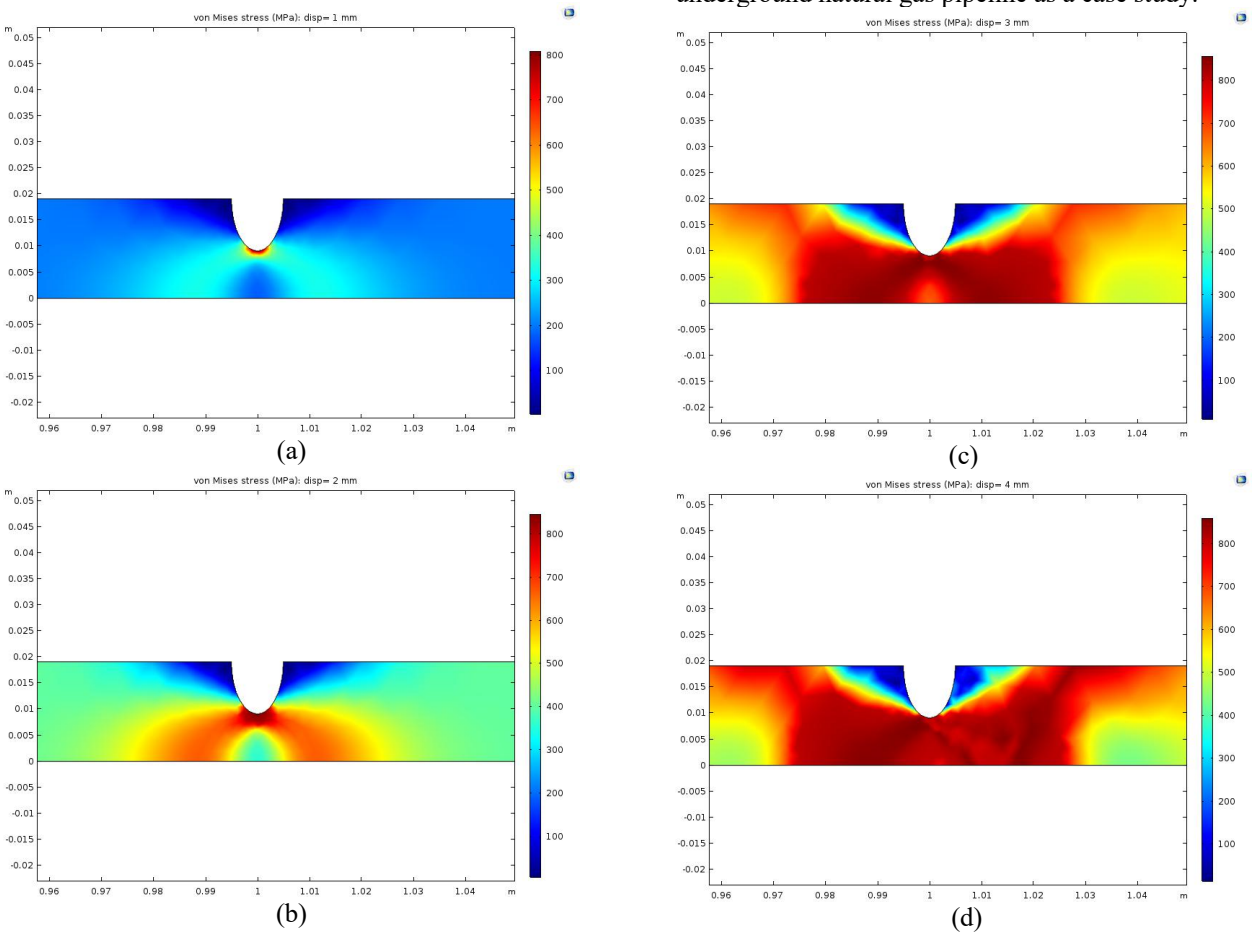

Figure 6. von Mises stress on the pipe under various longitudinal tensile strains: (a) 1 mm, (b) 2 mm, (c) 3 mm, and (d) 4 mm.

4. Simulation Results

4.1 Stress Corrosion Cracking (SCC) model

This section provides the results of the SCC simulations described in the previous sections. The results aim at showing the effect of different strains and different defect depths and lengths on von Mises stress and corrosion potential.

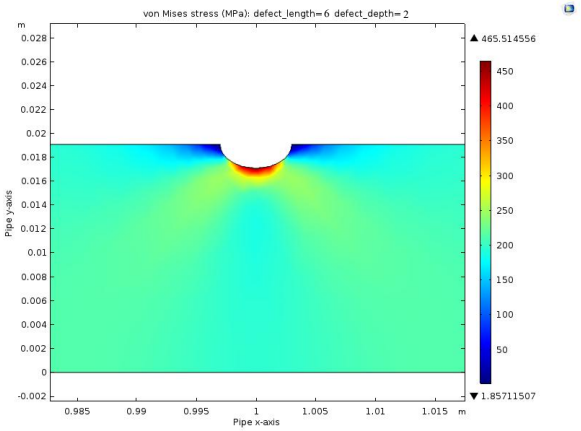

(a)

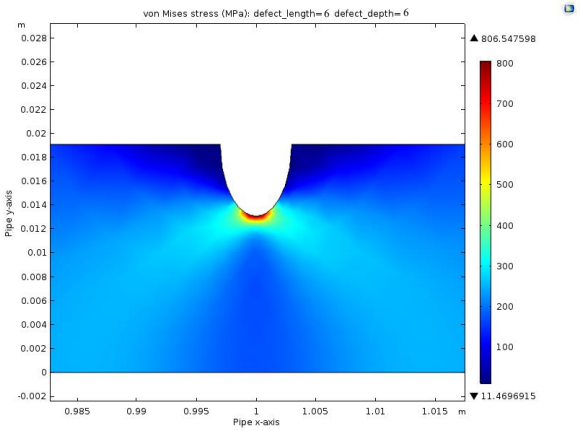

(b)

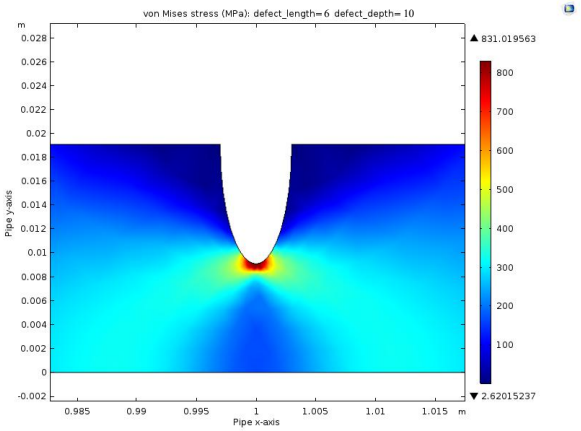

(c)

Figure 7. von Mises stress under different defect depths: (a) 2 mm, (b) 6 mm, and (c) 10 mm.

In other words, the purpose of the simulation results analysis is to find an understanding of the effect of soil strain and defect size on the corrosion rate of the pipeline. The detailed results of sensitivity analysis of SCC model are shown in the Appendix Table A5.

4.1.1 Von Mises Stress

Figure 6 shows the von Mises stress distribution in MPa on the pipe under various longitudinal tensile strains. The strain is simulated by inducing different soil displacements. It can be seen that the stress is larger at the defect location compared to the rest of the pipeline domain.

In addition, stress increases significantly when the soil strain applied increases as well as the propagation length. For instance, at a location of 1.05 m in the x direction, the stress felt is negligible when the soil displacement is 1 mm, is around 400 MPa when the displacement is 2 mm, is around 600 MPa when the displacement is 3 mm, and is around 700 MPa when the displacement is 4 mm. These results show that the effect of the soil strain on the defect location as well as on the rest on the pipe is not negligible.

Figure 7 shows the von Mises stress under different defect depths and at a fixed defect length of 6 mm. This sensitivity analysis aims at understanding the effect of the stress on the pipe under different defect depths. It can be seen that the increase in the corrosion defect depth increases the stress at the bottom edge of the defect but decreases in the surface of the pipe. The stress seems to concentrate in the defect location and have a more significant effect on the inside of the pipe rather than the surface area.

4.1.2 Corrosion Potential

Figure 8 shows the corrosion potential under different defect depths and at a fixed defect length of 6 mm. This sensitivity analysis aims at understanding the corrosion potential variation under different defect depths. It can be seen that the increase in the corrosion defect depth decreases the corrosion potential at the bottom edge of the defect.

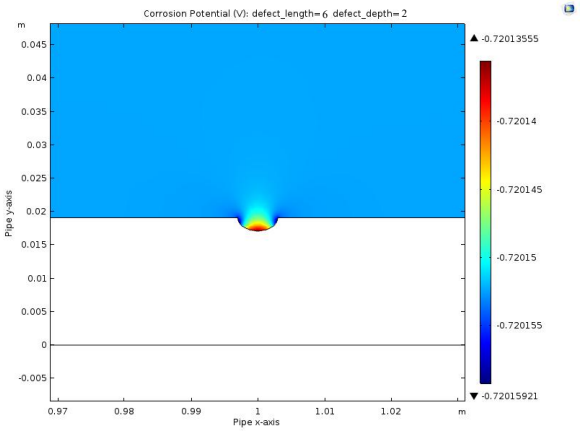

(a)

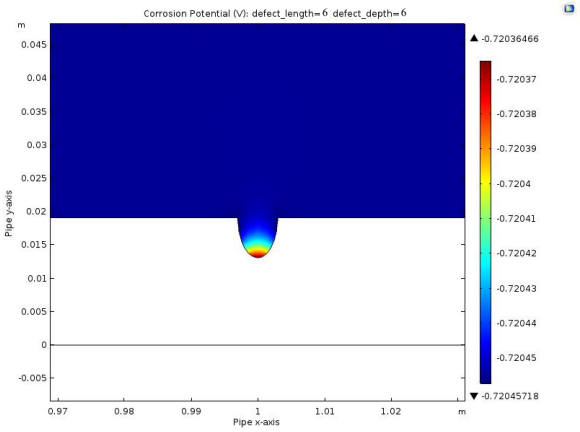

(b)

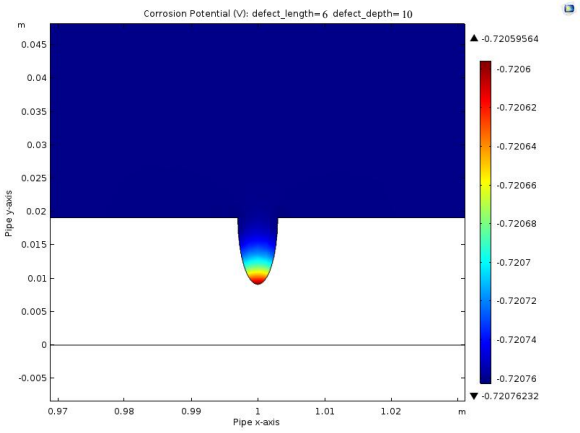

(c)

Figure 8. Corrosion potential under different defect depths: (a) 2 mm, (b) 6 mm, and (c) 10 mm.

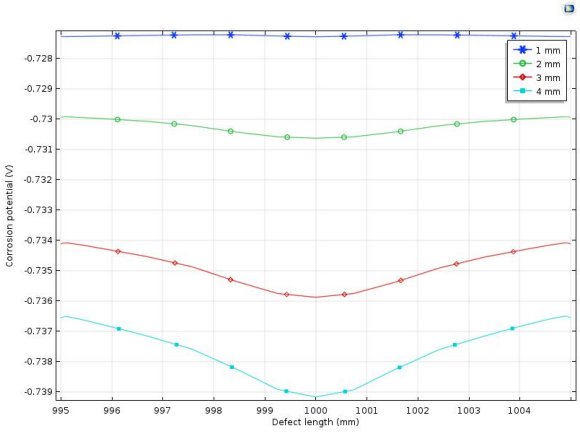

Figure 9. Linear distribution of corrosion potential along the length of the corrosion defect (length and depth of 5 mm) under various longitudinal tensile strains: soil displacements of 1, 2, 3, and 4 mm.

Figure 9 shows the distribution of the corrosion potential along the length of the corrosion defect under various longitudinal tensile strains: soil displacements of 1, 2, 3, and 4 mm. For this simulation, the defect length and depth were fixed at 10 mm. It is shown that for the smaller tensile strains of 1 and 2 mm, the variation in the corrosion potential is almost uniform along the length of the corrosion defect. However, for higher tensile strains of 3 and 4 mm, the variation in the corrosion potential is clearly nonuniform with the more negative corrosion potential at the center of the corrosion defect than that at both the sides of the corrosion defect.

Figure 10 shows the linear distribution of anodic current density (iron dissolution) along the length of the corrosion defect under various longitudinal tensile strains: soil displacements of 1, 2, 3, and 4 mm. For lower soil displacements of 1 mm and 2 mm, the anodic current density is almost uniform along the length of the corrosion defect, with an increase around the defect center. However, for higher soil displacements of 3 mm and 4 mm, the anodic current density varies and is significantly nonuniform, especially at the center of the corrosion defect. The increase in the anodic current density for higher strains could be explained by the plastic deformation observed at the center of the corrosion defect.

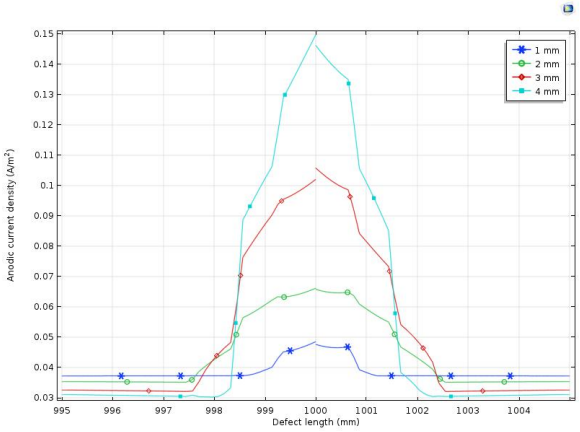

Figure 10. Linear distribution of anodic current density along the length of the corrosion defect under various longitudinal tensile strains: soil displacements of 1, 2, 3, and 4 mm.

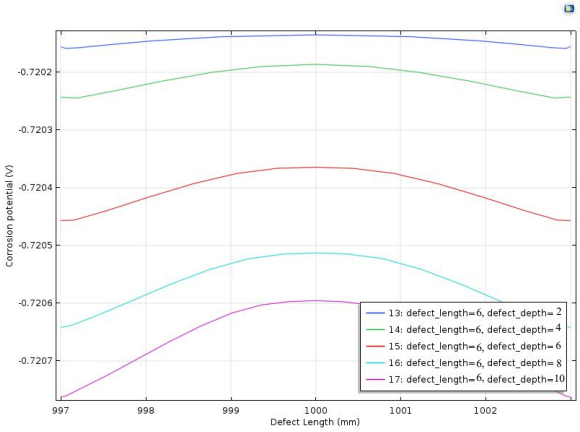

Figure 12. Linear distribution of corrosion potential along the bottom of corrosion defect with a fixed length of 3 mm and with various depths.

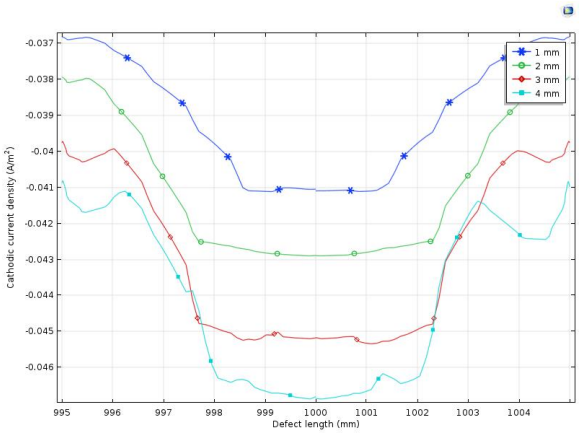

Figure 11. Linear distribution of cathodic current density along the length of the corrosion defect under various longitudinal tensile strains: soil displacements of 1, 2, 3, and 4 mm.

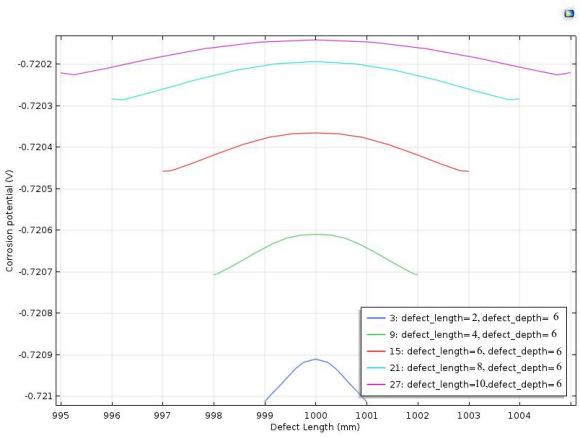

Figure 13. Linear distribution of corrosion potential along the bottom of corrosion defect with a fixed depth of 3 mm and with various lengths.

Figure 11 shows the linear distribution of cathodic current density (hydrogen evolution) along the length of the corrosion defect under various longitudinal tensile strains: soil displacements of 1, 2, 3, and 4 mm. This figure shows that the increase in the tensile strain decreases the cathodic current density, especially at the center of the corrosion defect where it is the most negative. Similar to the anodic current density distribution results, the nonuniformity in the cathodic current density increases when the tensile strain increases.

Figure 12 shows the linear distribution of corrosion potential along the bottom of corrosion defect with a length of 6 mm and with various depths where a 1 mm longitudinal tensile strain is applied. This figure shows that the increase of the defect depth decreases the corrosion potential along the defect location. In addition, it is shown that at low defect depths of 2 and 4 mm, the corrosion potential distribution is almost uniform. However, when the defect depth increases to 6, 8, and 10 mm, the corrosion potential is not uniform anymore with the highest corrosion potential at the center of the defect.

Figure 13 shows the linear distribution of corrosion potential along the bottom of corrosion defect with a fixed depth of 6 mm and with various lengths where a 1 mm longitudinal tensile strain is applied. This figure shows that the increase of the defect length increases the corrosion potential along the defect location.

4.2 Pitting Corrosion model

This section provides the results of the pitting corrosion simulations described in the previous sections. The purpose of this section is to demonstrate the capability of this model by showing the predicted pitting corrosion rate and depth given soil and pipe characteristics. A set of field data of underground gas pipelines collected across southern Mexico including soil and pipe data were used for demonstration (partly from [11]). Table 3 lists the data in a Distribution Type (mean, variance) format for every variable except for the coating type which is a constant. Monte Carlo (MC) simulation method was used to estimate the corrosion predictions in terms of rate and depth.

Table 3. Soil and pipe data of underground gas pipelines collected across southern Mexico

Variable, symbol (units)	Probability function
Resistivity, re (Ω-m)	Lognormal (50, 2931)
Sulphate, sc (ppm)	Lognormal (154, 25328)
Bicarbonate, bc (ppm)	Lognormal (19, 436)
Chloride, cc (ppm)	Lognormal (41, 3135)
Water content, wc(%)	Normal (24, 38)
pH, ph	Gumbel (6.13, 0.84)
Pipe/soil potential, pp (V)[1]	Normal (-0.86, 0.04)
Bulk density, bd (g/ml)	Normal (1.30, 0.007)
Redox potential, rp (mV)[2]	Uniform (2.14, 348)
	Deterministic function
Coating type, ct	Constant (0.7651)
Operating time, t	Constant (20)

[1] Relative to a Cu/CuSO4 reference electrode.
[2] Relative to the standard hydrogen electrode.

4.2.1 Pitting Rate

Figure 14 displays the distribution of pitting rate for underground gas pipelines after 20 years of operation. The distribution has a long tail in high pitting rate region in a reflection of the uncertainties of soil and pipe parameters. Although the mean pitting rate is roughly 0.03 mm/y, the maximum pitting rate can be as high as 0.27 mm/y.

4.2.2 Pitting Depth

Figure 15 displays the distribution of maximum pitting depth for underground gas pipelines after 20 years of operation. As pitting depth is the accumulative consequence of pitting rate over time, the distribution also has a long tail in high maximum pitting depth region. The mean maximum pitting depth is 0.96 mm, but the maximum pitting depth is as high as 7.08 mm. Although the maximum pitting depth is less likely to happen, it should still be treated seriously because the location with the highest pitting is usually where the failure happens.

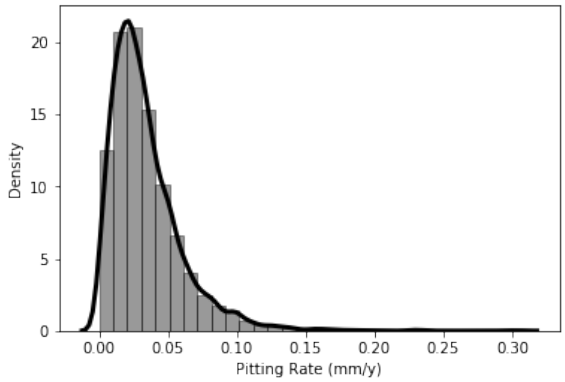

Figure 14. Distribution of pitting rate for underground gas pipelines after 20 years of operation.

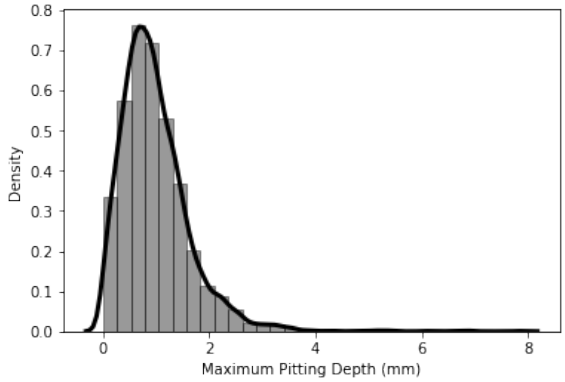

Figure 15. Distribution of maximum pitting depth for underground gas pipelines after 20 years of operation.

4.3 External Corrosion BN model

A cause-consequence relationship external corrosion model was developed to predict external corrosion considering both SCC and pitting corrosion as shown in Figure 5. A small portion of the external corrosion BN model was highlighted and shown in Figure 16 to illustrate how the model works. The conditional probability table was developed by the models for SCC and pitting corrosion described in this paper and expert knowledge. The comprehensive details of each discretized node in the BN model were listed in the authors' previous work for reader's reference [2].

An example of the Bayesian calculations shown in Figure 16 are displayed in Table 4. All nodes in this BN model are discrete. Also, the states for each node are uniformly distributed. The results shows that when the coating type is more likely to be coal-tar with 44.3% probability; pipe-soil potential is more likely to between -1.0 to -0.5 V with 72.1% probability; bulk density is more likely to between 1 to 1.5 g/ml with 99.1% probability; water content is more likely to be between 0 to 25% with 56.9% probability; the exponent of the pitting model is likely to be between 0.5 to 0.75 with 73.5% probability.

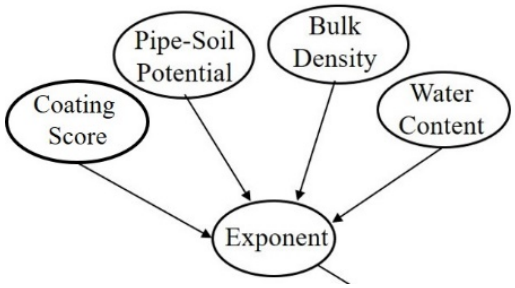

Figure 16. A small portion of the external corrosion BN model.

Table 4. Results of Bayesian calculation for Figure 16

Parameters	Value	Certainty (%)
Coating type	Bare pipe Asphalt enamel Wrap-tape Coal-tar FBE	11.8 2.4 38.2 44.3 3.3
Pipe-to-soil potential (V)	(-2.0)-(-1.5) (-1.5)-(-1.0) (-1.0)-(-0.5) (-0.5)-0	0.1 23.9 72.1 3.9
Bulk density (g/ml)	0-0.5 0.5-1 1-1.5 1.5-2	0 0.1 99.1 0.8
Water content (%)	0-25 25-50 50-75 75-100	56.9 43.1 0 0
Exponent	0-0.25 0.25-0.5 0.5-0.75 0.75-1	0 6.5 73.5 20

The same treatment was performed for the other nodes in a cause-consequence relationship. The overall model tracks much more nodes than the demonstrated one; each of which has direct or indirect effects on external corrosion. The comprehensive details of each node in the BN model were listed in the authors' previous work for reader's reference [2].

5. Case Study

For the sake of model demonstration on an operating underground gas pipeline subject to external corrosion, the developed external corrosion BN model was used to calculate the corrosion rate and depth of an underground gas pipeline via a case study. The experimental data available in the references [8, 11] are used. The pipeline is 1000 km in length and 10 mm in thickness. The type of the pipe material is X100 pipeline steel. Only coating is applied to the pipeline as a protection against external corrosion, and it has been operating for 20 years. Due to the lack of information regarding corrosion initiation time, it was assumed that the corrosion defect started to grow after the pipeline was operated. In addition, it should be noted that the SCC model developed in COMSOL Multiphysics can be used to predict the corrosion rate but not the corrosion depth. Therefore, the corrosion defect as a result of SCC was assumed to grow linearly with respect to time for simplicity. For external corrosion, leakage is considered a most common failure; therefore, the probability of failure due to leakage was calculated assuming the leakage will happen when 80% of the wall thickness is lost due to corrosion. The inputs for the external corrosion BN model are summarized in Table 5.

Table 5. Soil and pipe data of a demonstrative underground gas pipeline subject to external corrosion

Parameters	Value	Certainty (%)
Coating type	Bare pipe Asphalt enamel Wrap-tape Coal-tar FBE	11.8 2.4 38.2 44.3 3.3
Pipe-to-soil potential (V)	(-2.0)-(-1.5) (-1.5)-(-1.0) (-1.0)-(-0.5) (-0.5)-0	0.1 23.9 72.1 3.9
Bulk density (g/ml)	0-0.5 0.5-1 1-1.5 1.5-2	0 0.1 99.1 0.8
Water content (%)	0-25 25-50 50-75 75-100	56.9 43.1 0 0
Soil resistivity (Ω-m)	1-250 250-500 500-750 750-1000	99.94 0.04 0.02 0
Sulphate content (ppm)	0-10 10-100 100-1000 1000-2500	0.44 39.28 58.52 1.76
Bicarbonate content (ppm)	0-10 10-100 100-1000 1000-4000	29.12 69.58 1.30 0

Chloride content (ppm)	0-100 100-1000 1000-10000 10000-100000	89.88 10.12 0 0
pH	4-5 5-6 6-7 7-8 8-9	0 4.74 45.34 34.86 15.06
Redox potential	1-100 100-200 200-300 300-400	28.40 35.58 35.66 0.36
Cathodic i_0[1] (A/m^2)	(-10^{-4}) – (-10^{-3}) (-10^{-3}) – (-10^{-2}) (-10^{-2}) – (-10^{-1}) (-10^{-1}) – (-1)	0 50 50 0
Anodic i_0[1] (A/m^2)	10^{-4} – 10^{-3} 10^{-3} – 10^{-2} 10^{-2} – 10^{-1} 10^{-1} – 1	50 50 0 0
Defect Depth (mm)	0-0.1 0.1-1 1-10 10-20	0 55 45 0
Defect Length (mm)	0-0.1 0.1-1 1-10 10-20	0 55 45 0
Strain/Displacement[2] (mm)	10^{-2} – 10^{-1} 10^{-1} – 1 1 – 10	0 50 50

[1] Cathodic i_0 and Anodic i_0 are exchange cathodic current density and exchange anodic current density respectively, which are related to operating conditions such as temperature, pH, etc.

[2] Strain/Displacement is the longitudinal strain of the pipe due to soil movements.

The results of the demonstrative gas pipeline are shown in Table 6. The corrosion rate is likely to fall into the range between 0.01 to 0.1 mm/y, while the corrosion depth is likely to fall into the range between 1 to 5 mm after 20 years of operation. The pipe is not in urgent demand for repair at this time as there are 99% chance that the probability of failure due to leakage is under 20%.

The developed BN model can be easily applied to other similar gas pipelines for external corrosion prediction because although the development of conditional probability tables of the BN model requires hundreds to thousands of simulations, once it is generated no more simulation is needed. There are several advantages including that if evidence of a node is available (certainty is 100%), the predictive result can then be updated. On the other hand, even though the information of a certain node is unavailable, BN model can simply take the uncertainty into account by assigning all values of that node with equal probabilities. In addition, the cause-consequence relationship feature allows it to integrate many kinds of data, namely, physics-based model, field data, expert knowledge, and literature data, among which the physics-based model is more reliable but also rare and that is the motivation that this paper uses COMSOL Multiphysics to generate physics-based simulation data of SCC.

Table 6. Results of Bayesian calculation for a demonstrative underground gas pipeline subject to external corrosion

Parameters	Value	Certainty (%)
External Corrosion Rate (mm/y)	0-0.01 0.01-0.1 0.1-1 1-5 5-10	0.25 99.34 0.41 0 0
External Corrosion Depth (mm)	0-0.1 0.1-1 1-5 5-10 10-20	0. 0 99 1 0
Probability of Failure due to leakage (%)	0-20 20-40 40-60 60-80 80-100	99 0.51 0.49 0 0

6. Conclusions

In conclusion, this paper presented an external corrosion modeling for an underground natural gas pipeline subject to Stress Corrosion Cracking (SCC) and pitting corrosion. For the SCC, the model is implemented using the Solid Mechanics and the Secondary Current Distribution interfaces in COMSOL Multiphysics. This model studied the impact of elastoplastic deformations on electrochemical reactions. It was shown that the maximum corrosion potential along the defect length decreases with the increasing defect depth, but increases with increasing defect length, and that the maximum von Mises stress increases with increasing defect depth but decreases with increasing defect length, which indicates that the corrosion is most severe at the center of the defect. That trend can also be seen by quantifying the corrosion level into

corrosion rate. For the pitting corrosion, the applied pitting corrosion model is able to predict the pitting corrosion rate given soil and pipe data at different types of soil conditions. Finally, the proposed BN model considering both SCC and pitting corrosion has shown its potential in predicting external corrosion rate and depth of underground gas pipelines. The advantages such as flexibility of updating with evidence and ability of taking uncertainty of inputs makes the model more flexible and easier for field application to aid decision makings.

Acknowledgements

The authors would like to acknowledge the sponsorship of the Petroleum Institute, Khalifa University of Science and Technology, Abu Dhabi, UAE and the University of Maryland (Department of Mechanical Engineering) for the research work presented in this paper, which is part of the Pipeline System Integrity Management research project. In addition, the authors would like to acknowledge the SEAS-net Computing Facility and UCLA for proving the license to use COMSOL Multiphysics, which supported the numerical study.

References

[1] O.Shabarchin andS.Tesfamariam, "Internal corrosion hazard assessment of oil & gas pipelines using Bayesian belief network model," *J. loss Prev. Process Ind.*, vol. 40, pp. 479–495, 2016.

[2] W.Chalgham, M.Diaconeasa, K.-Y.Wu, andA.Mosleh, "A Dynamic Pipeline Network Health Assessment Software Platform for Optimal Risk-based Prioritization of Inspection, Structural Health Monitoring, and Proactive Management," *Proceedings of the ASME 2019, International Mchanical Engineering Congress and Exposition IMECE2019*, November 11-14, 2019, Salt Lake City, UT, USA.

[3] K. Y.Wu andA.Mosleh, "Effect of Temporal Variability of Operating Parameters in Corrosion Modelling for Natural Gas Pipelines Subjected to Uniform Corrosion," *J. Nat. Gas Sci. Eng.*, p. 102930, 2019.

[4] S.Papavinasam, A.Doiron, andR. W.Revie, "Model to predict internal pitting corrosion of oil and gas pipelines," *Corrosion*, vol. 66, no. 3, pp. 35006–35011, 2010.

[5] S.Nešic andJ.Postlethwaite, "A predictive model for localized erosion—corrosion," *Corrosion*, vol. 47, no. 8, pp. 582–589, 1991.

[6] B. F. M.Pots *et al.*, "Improvements on de Waard-Milliams corrosion prediction and applications to corrosion management," in *CORROSION 2002*, 2002.

[7] K.Zaman andR. P.Wei, "Probability approach for prediction of corrosion and corrosion fatigue life," *AIAA J.*, vol. 32, no. 10, pp. 2073–2079, 1994.

[8] L. Y.Xu andY. F.Cheng, "Development of a finite element model for simulation and prediction of mechanoelectrochemical effect of pipeline corrosion," *Corros. Sci.*, vol. 73, pp. 150–160, 2013.

[9] L.Xu, "Assessment of corrosion defects on high-strength steel pipelines." University of Calgary, 2013.

[10] J. C.Velázquez, F.Caleyo, A.Valor, andJ. M.Hallen, "Predictive model for pitting corrosion in buried oil and gas pipelines," *Corrosion*, vol. 65, no. 5, pp. 332–342, 2009.

[11] F.Caleyo, J. C.Velázquez, A.Valor, andJ. M.Hallen, "Probability distribution of pitting corrosion depth and rate in underground pipelines: A Monte Carlo study," *Corros. Sci.*, vol. 51, no. 9, pp. 1925–1934, 2009.

Appendix

Table A1. High-strength alloy steel material properties

Name	Value	Unit
Density	7850	kg/m³
Young's modulus	207e9	Pa
Poisson's ratio	0.33	
Initial yield stress	806e6	Pa
Relative permeability	{{1, 0, 0}, {0, 1, 0}, {0, 0, 1}}	
Heat capacity at constant pressure	475	J/(kg*K)]
Thermal conductivity	{{44.5, 0, 0}, {0, 44.5, 0}, {0, 0, 44.5}}	W/(m*K)
Electrical conductivity	{{4.032e6, 0, 0}, {0, 4.032e6, 0}, {0, 0, 4.032e6}}	S/m
Relative permittivity	{{1, 0, 0}, {0, 1, 0}, {0, 0, 1}}	
Coefficient of thermal expansion	{{12.3e-6, 0, 0}, {0, 12.3e-6, 0}, {0, 0, 12.3e-6}}	1/K
Lamé parameter λ	1.15e11	Pa
Lamé parameter μ	7.69e10	Pa

Table A2. Parameters used for the simulation

Name	Expression	Value	Description
disp	0.001 [m]	0.001 m	Displacement
Eeq0_fe	-0.859 [V]	−0.859 V	Equilibrium potential for iron dissolution vs SCE in absence of stress
Eeq0_h	-0.644[V]	−0.644 V	Equilibrium potential for hydrogen evolution vs SCE in absence of stress
i0a	2.353e-3[A/m^2]	0.002353 A/m²	Exchange current density for iron dissolution
ba	118[mV]	0.118 V	Tafel slope for iron dissolution
i0c_h	1.457e-2[A/m^2]	0.01457 A/m²	Exchange current density for hydrogen evolution
bc	-207[mV]	−0.207 V	Tafel slope for hydrogen evolution
deltaPm	806e6[Pa]/3	2.6867E8 Pa	Excess pressure to elastic deformation
Vm	7.13e-6 [m^3/mol]	7.13E−6 m³/mol	Molar volume of steel
zm	2	2	Charge number
T	298.15[K]	298.15 K	Temperature
nu	0.45	0.45	Orientation dependent factor
alpha	1.67e11[1/cm^2]	1.67E15 1/m²	Coefficient
N0	1e8[1/cm^2]	1E12 1/m²	Initial dislocation density
deltaEeqae	-(deltaPm*Vm/(zm*F_const))	−0.0099269 V	Change in equilibrium potential due elastic deformation
sigmal	0.096 [S/m]	0.096 S/m	Soil conductivity
defect_depth	5 [mm]	0.005 m	Initial defect depth
defect_length	5 [mm]	0.005 m	Initial defect length

Table A3. Variables used for the simulation

Name	Expression	Unit	Description
hardening	max(0,stress_strain_curve(solid.epe+solid.mises/solid.E) - solid.sigmags)	Pa	Hardening function
deltaEeqap	-T*R_const/(zm*F_const)*log((nu*alpha*solid.epe)/N0 + 1)	V	Change in anode equilibrium potential due plastic deformation
Eeqa	Eeq0_fe+deltaEeqae+deltaEeqap	V	Anode equilibrium potential including elastic and plastic deformation terms
ic_h	i0c_h*10^(-solid.mises*Vm/(6*F_const*bc))	A/m²	Cathode exchange current density including stress factor

Table A4. Mesh Properties

Description	Value
Minimum element quality	0.6912
Average element quality	0.9424
Triangle	6013
Edge element	697
Vertex element	9
Maximum element size for the soil domain	0.067
Minimum element size for the soil domain	3.0E-4
Curvature factor	0.3
Maximum element growth rate	1.3
Maximum element size for the pipeline domain	0.002
Minimum element size for the pipeline domain	6.0E-4

Table A5. Results of sensitivity analysis of SCC model for fixed cathodic i_0 at 0.01457 A/m^2 and fixed anodic i_0 at 0.002353 A/m^2 where the defect length and depth were varied

Simulation #	Displacement (mm)	Defect length (mm)	Defect depth (mm)	Anodic current density (A/m^2)	Cathodic current density (A/m^2)	Maximum corrosion potential (V)	Corrosion rate (mm/y)
1	1	2	2	0.0351	-0.0381	-0.7204	0.0409
2	2	2	2	0.0354	-0.0382	-0.7201	0.0411
3	3	2	2	0.0355	-0.038	-0.7199	0.0412
4	1	2	4	0.0349	-0.0382	-0.7208	0.0405
5	1	2	6	0.0348	-0.0383	-0.7209	0.0404
6	1	2	8	0.0347	-0.0385	-0.7209	0.0404
7	1	2	10	0.0347	-0.0386	-0.7210	0.0404
8	2	2	10	0.0349	-0.0383	-0.7207	0.0406
9	3	2	10	0.0349	-0.0382	-0.7207	0.0405
10	1	2	16	0.0349	-0.0384	-0.720	0.0406
11	1	4	2	0.0353	-0.037	-0.7201	0.0410

12	1	4	4	0.0351	-0.038	-0.7204	0.0409
13	1	4	6	0.0350	-0.0382	-0.7206	0.0407
14	1	4	8	0.0349	-0.0383	-0.7207	0.0406
15	1	4	10	0.0349	-0.0384	-0.7208	0.0405
16	1	6	2	0.0353	-0.0363	-0.7201	0.0411
17	1	6	4	0.0353	-0.03775	-0.7202	0.0410
18	1	6	6	0.0351	-0.038	-0.7204	0.0409
19	1	6	8	0.0350	-0.003825	-0.7205	0.0408
20	1	6	10	0.0350	-0.0385	-0.7206	0.0407
21	1	8	2	0.0353	-0.036	-0.7201	0.0410
22	1	8	4	0.0353	-0.037	-0.7201	0.0410
23	1	8	6	0.0353	-0.0378	-0.7202	0.0410
24	1	8	8	0.0352	-0.038	-0.7203	0.0409
25	1	8	10	0.0351	-0.03825	-0.7204	0.0408
26	1	10	2	0.0353	-0.03555	-0.7201	0.0410
27	1	10	4	0.0353	-0.0365	-0.7201	0.0411
28	1	10	6	0.0353	-0.0375	-0.7201	0.0410
29	1	10	8	0.0353	-0.038	-0.7202	0.0410
30	1	10	10	0.0352	-0.0382	-0.7203	0.0409
31	1	20	2	0.0352	-0.0354	-0.7203	0.0409
32	2	20	2	0.0360	-0.0364	-0.7191	0.0418
33	3	20	2	0.0368	-0.0371	-0.7181	0.0427

Table A6. Results of sensitivity analysis of SCC model for fixed defect length and depth of 6 mm and fixed displacement of 1 mm where the exchange anodic and cathodic current densities were varied

Simulation #	**Exchange anodic current density (A/m^2)**	**Exchange cathodic current density (A/m^2)**	**Corrosion Potential (V)**	**Anodic current density (A/m^2)**	**Cathodic current density (A/m^2)**	**Corrosion rate (mm/y)**
1	0.001353	0.00457	-0.7402	0.0137	-0.0151	0.0159
2	0.001353	0.01457	-0.7023	0.0288	-0.0311	0.0334
3	0.001353	0.02457	-0.6852	0.0401	-0.0438	0.0466
4	0.002353	0.00457	-0.7582	0.0168	-0.0183	0.0195
5	0.002353	0.01457	-0.7204	0.0351	-0.0384	0.0408
6	0.002353	0.02457	-0.7033	0.0490	-0.0538	0.0569
7	0.003353	0.00457	-0.7698	0.0191	-0.0214	0.0222
8	0.003353	0.01457	-0.7319	0.0399	-0.0432	0.0463
9	0.003353	0.02457	-0.7148	0.0557	-0.0611	0.0647